



# Synthesis of $\gamma$ -graphyne using dynamic covalent chemistry

Yiming Hu<sup>1</sup>, Chenyu Wu<sup>2</sup>, Qingyan Pan<sup>2</sup>, Yinghua Jin<sup>1</sup>, Rui Lyu<sup>3</sup>, Vikina Martinez<sup>4</sup>, Shaofeng Huang<sup>1</sup>, Jingyi Wu<sup>1</sup>, Lacey J. Wayment<sup>1</sup>, Noel A. Clark<sup>4</sup>, Markus B. Raschke<sup>3</sup>, Yingjie Zhao<sup>2</sup>✉ and Wei Zhang<sup>1</sup>✉

**Most attempts to synthesize graphynes are limited to using irreversible coupling reactions, which often result in the formation of nanometre-scale materials that lack long-range order. Here the periodically  $sp$ - $sp^2$ -hybridized carbon allotrope,  $\gamma$ -graphyne, was synthesized in bulk via a reversible dynamic alkyne metathesis of alkynyl-substituted benzene monomers. The balance between kinetic and thermodynamic control was managed through the simultaneous use of two different hexa-alkynyl-substituted benzenes as the comonomers to yield crystalline  $\gamma$ -graphyne. Additionally, the ABC staggered interlayer stacking of the graphyne was revealed using powder X-ray and electron diffraction. Finally, the folding behaviour of the few-layer graphyne was also observed on exfoliation, and showed step edges within a single graphyne flake with a height of 9 nm.**

Carbon atoms can be  $sp^3$ -,  $sp^2$ - or  $sp$  hybridized to form single, double or even triple bonds with neighbouring carbon atoms and so produce various allotropes. The most well-known carbon allotropes are graphite and diamond, which are made of purely  $sp^2$ - and  $sp^3$ -hybridized carbon atoms, respectively. Carbon allotropes have distinct physical properties that arise from the unique combination and arrangement of multiple types of bonds that have various length, strength, geometry and electronic properties. For instance, graphite is opaque and soft, whereas diamond is transparent and the hardest known natural substance. Tremendous research efforts have been devoted to constructing novel carbon allotropes, which include  $sp^2$ -hybridized carbon allotropes, fullerene (awarded the Nobel Prize in Chemistry in 1996)<sup>1</sup>, carbon nanotubes<sup>2</sup>, graphene (awarded Nobel Prize in Physics in 2010)<sup>3</sup>, a biphenylene network<sup>4</sup> and an  $sp$ -hybridized carbon allotrope, cyclo[18]carbon<sup>5</sup>. All of the above known carbon allotropes are composed of a single type of carbon atom. However, there are many more composed of various combinations of  $sp^3$ -,  $sp^2$ - and  $sp$ -hybridized carbon atoms and yet to be discovered.

Graphynes are two-dimensional (2D) carbon allotropes similar to the wonder material graphene that is optically transparent and mechanically flexible, and yet strong and electronically conductive. The discovery of graphene ushered in a new era of 2D materials and quantum technology. Unlike graphenes, which consist solely of  $sp^2$ -hybridized carbons, graphynes contain  $sp$ -hybridized carbons periodically integrated into an  $sp^2$ -hybridized carbon framework (Fig. 1a). It was predicted that graphyne would exhibit intriguing and unique electron-conducting<sup>6–8</sup>, mechanical<sup>9–11</sup> and optical<sup>8</sup> properties. Specifically, the electron conduction in graphynes would be exceptionally fast, as it is in graphene<sup>6,7</sup>. Yet, the electron conduction in some graphynes could be controlled in a defined direction, unlike the multidirectional conduction in graphene, because the triple bonds can create distortion in Dirac cones<sup>12,13</sup>. A variety of low-molecular-weight graphyne fragments or ethynylene-linked molecular architectures, which include carbyne,

were synthesized by the groups of Haley<sup>14–16</sup>, Tykwinski<sup>17–19</sup>, Nielsen<sup>17</sup>, Tobe<sup>20–22</sup> and Moore<sup>20,23</sup>, to name a few, and showed attractive optoelectronic and self-assembly properties<sup>24–26</sup>. Most attempts to synthesize graphynes are limited to using irreversible coupling reactions, such as the Glaser–Hay coupling, on a copper surface or air–water interfaces. This approach was used to form nanometre-scale graphdiyne and graphtetrayne, which lack long-range order<sup>27–30</sup>. Bulk-scale synthesis has also been attempted through an irreversible coupling between hexabromobenzene and calcium carbide, with limited success<sup>31–33</sup>. These attempts give tantalizing glimpses of graphyne families, but the large-scale synthesis of graphynes with long-range crystallinity over a large area remains elusive. Moreover, to the best of our knowledge, the most stable graphyne structure<sup>34</sup>,  $\gamma$ -graphyne, which consists of alternating phenylene ( $sp^2$ -hybridized carbons only) and ethynylene ( $sp$ -hybridized carbons only) building blocks, has not been fully experimentally realized. Additionally, the lack of knowledge on the stacking order and orientation of adjacent graphyne layers has impeded the study of graphyne properties.

Here we report the bulk synthesis of crystalline  $\gamma$ -graphyne in the solution phase and reveal its ‘ABC’ stacking in the crystal structure. Alkyne metathesis was used to reversibly cleave and reform the bonds between  $sp$ -hybridized carbon atoms as a dynamic covalent synthetic approach to obtain a crystalline  $\gamma$ -graphyne network. A meticulous balance between kinetic and thermodynamic control was managed through the simultaneous use of two types of hexa-alkynyl-substituted benzenes as the comonomers to achieve error correction and polymer network growth with periodicity. Few-layer  $\gamma$ -graphyne was obtained on exfoliation and the layered morphology was studied. Importantly, the multilayered stacking mode was fully characterized, which provides valuable insights into the  $\gamma$ -graphyne structure. We believe such stacking information is imperative to study the quantum phenomena of layered graphynes, which could rival the unexpected superconductivity observed in magic-angle bilayer<sup>35</sup> or trilayer graphenes<sup>36</sup>.

<sup>1</sup>Department of Chemistry, University of Colorado Boulder, Boulder, CO, USA. <sup>2</sup>College of Polymer Science and Engineering, Qingdao University of Science and Technology, Qingdao, China. <sup>3</sup>Department of Physics and JILA, University of Colorado, Boulder, CO, USA. <sup>4</sup>Department of Physics and Liquid Crystal Materials Research Center, University of Colorado, Boulder, CO, USA. ✉e-mail: yz@qust.edu.cn; wei.zhang@colorado.edu

## Results and discussion

Dynamic covalent chemistry has shown great success in constructing crystalline ordered polymeric architectures, which include single crystals of covalent organic frameworks<sup>38</sup> and helical covalent polymers<sup>39</sup> with long-range order over several tens of micrometres. To achieve a structural order in polymer networks, it is advantageous to employ a dynamic covalent reaction<sup>40</sup> and enable error correction under thermodynamic control. Retrosynthetic analysis of a phenylene–ethynylene fragment that consists of  $sp^2$ - and  $sp$ -hybridized carbons shows that there are two possible ways to construct the bonds. One forms the carbon–carbon single bond between the phenylene and ethynylene groups, and the other forms carbon–carbon triple bonds (Fig. 1b). Cross-coupling between an  $sp$ -hybridized carbon and an  $sp^2$ -hybridized carbon is an irreversible reaction and generally fails to provide bulk polymeric materials with low defect densities. On the contrary, alkyne metathesis is a reversible reaction and proceeds through either a non-productive pathway, in which the end groups are simply exchanged without forming any new chemical structures, or through a productive pathway, in which new products are formed, usually along with small alkyne by-products (for example, 2-butyne). The productive pathway and its reversibility enable both polymer growth and self-correction. We selected alkyne metathesis as the suitable dynamic covalent reaction to polymerize hexa-alkynyl benzene monomers to form  $\gamma$ -graphyne with a high crystallinity. To suppress the non-productive pathway and promote polymerization, the 2-butyne by-product was removed from the system to drive the equilibrium towards the polymer growth, based on Le Châtelier's principle. However, the presence of small alkyne by-products is also necessary for error correction, because they have a better mobility compared with that of the alkyne groups embedded in the polymer network and thus a greater chance to reversibly react with triple bonds on defect sites and reposition them into the correct spots.

We selected 1,2,3,4,5,6-hexapropynylbenzene (HPB) as the major monomer for the  $\gamma$ -graphyne synthesis. Alkyne metathesis of HPB produced 2-butyne as the by-product in the productive pathway. The low boiling point of 2-butyne allows its easy removal under a reduced pressure, which promotes the polymer growth. However, if the polymerization is fully driven by kinetic growth, the ordered structure is challenging to obtain, because kinetically trapped amorphous solids with undesired and disordered bond connections are predominantly formed. To facilitate the self-correction mechanism during the polymer growth, 1,2,3,4,5,6-hexakis[2-(4-hexylphenyl)ethynyl]benzene (HHEB) was added as a comonomer. HHEB provides the same repeating monomer unit as HPB, but instead of propynyl it has hexyl-substituted phenylethynyl as the end groups (Fig. 1c). There are several advantages of using HHEB monomers. First, the hexyl substituents dramatically increase the solubility of graphyne oligomers, which thus allow the materials to grow into larger ordered domains before they precipitate as the initial nuclei. Second, unlike 2-butyne, the by-product bis(4-hexylphenyl)acetylene has a comparable reactivity to that of the graphyne repeating unit. Therefore, there is a lower kinetic barrier for bis(4-hexylphenyl)acetylene to reversibly react with the graphyne fragment and correct the undesired bond formation with kinetically introduced disorder. Third, the backbone structure of HHEB mimics the repeating unit of  $\gamma$ -graphyne, which probably provides a templating

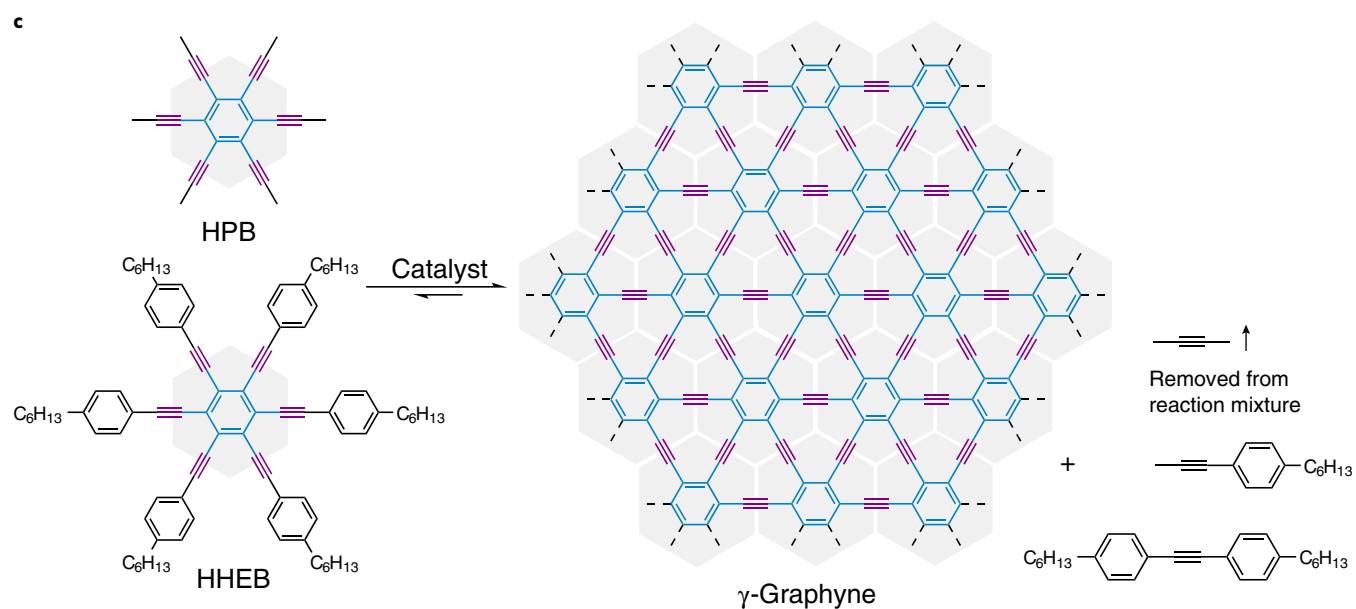
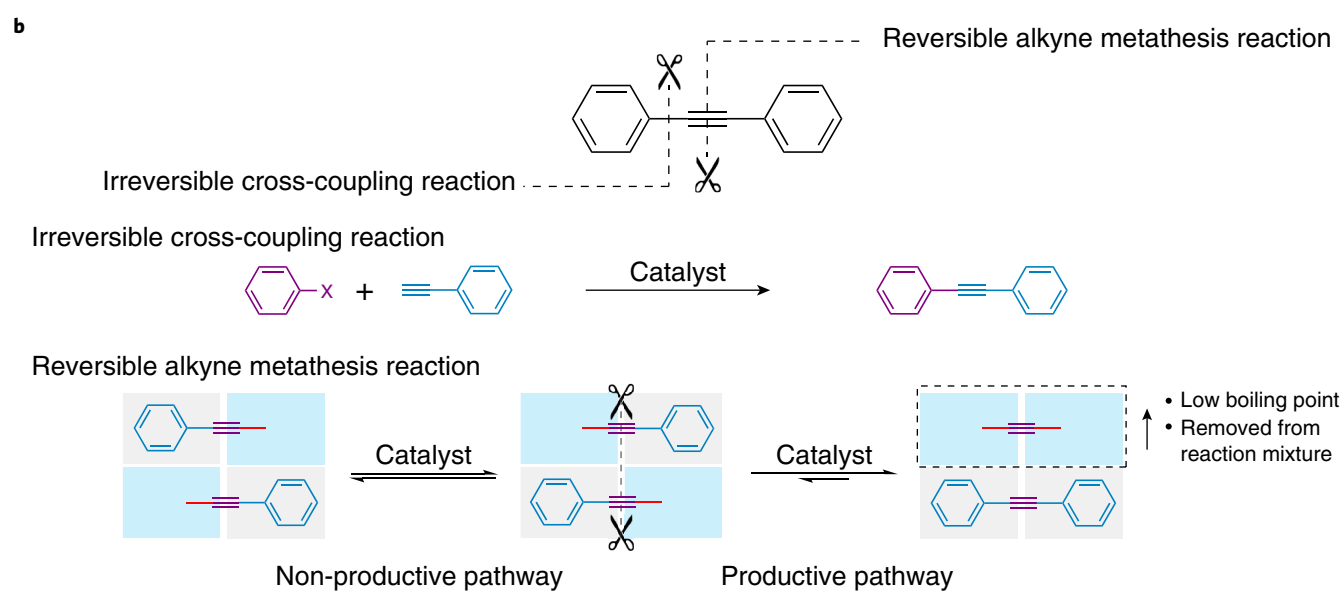
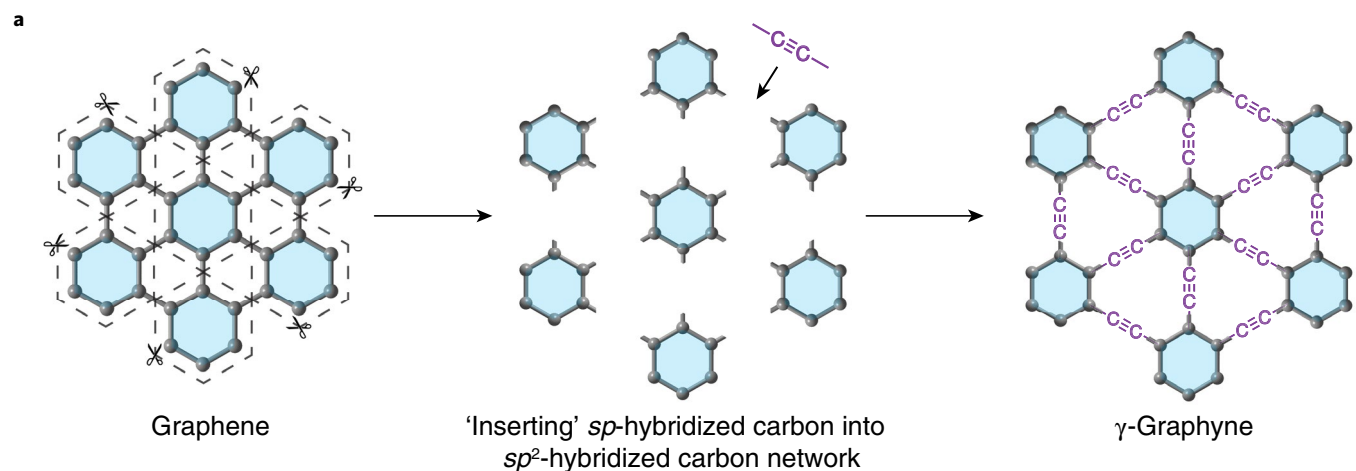
effect for the graphyne growth. Therefore, HHEB serves as a 'correction modulator' by increasing the reversibility of the alkyne metathesis and promoting self-correction. Note that a fine balance between HPB and HHEB amount is critical. When HPB was used as the sole monomer, only an amorphous solid was obtained, whereas with an excess of the correction modulator (HHEB), the polymer growth was inhibited and only soluble short oligomers were formed due to the predominant non-productive pathway (loss of the driving force). After carefully screening a series of mixtures of HPB and HHEB from 100% to 0%, we found that the optimum ratio was 90% HPB and 10% HHEB. HPB provides the driving force for polymerization and crystalline domain growth, whereas HHEB promotes the self-correction and formation of the ordered framework structure. Under the optimum conditions with the periodic removal of the 2-butyne by-product, the  $sp$ - $sp^2$ -hybridized graphyne with a crystalline ordered structure was obtained as a dark black precipitate from the solution in a good yield of 72%. We used a Mo(VI) alkyne metathesis catalyst<sup>41</sup> with a high stability, long lifetime and high catalytic efficiency.

The as-synthesized  $\gamma$ -graphyne was first characterized with optical microscopy (Fig. 2a). A dispersion of the graphyne thin films in acetone was transferred to isopropyl alcohol, sonicated and drop cast onto a 100 nm  $\text{SiO}_2/\text{Si}$  wafer. The dark reflection on the optical microscopy image suggests the existence of a large-area thin-layered film. The corresponding graphyne flake was further characterized with ambient atomic force microscopy (AFM) to determine the film thickness, size and homogeneity. Ambient AFM confirmed layered films with steps of around 10 nm, which corresponds to about 30 layers of  $\gamma$ -graphyne stacked together. We also observed a free-standing flake with an area over  $10\ \mu\text{m}^2$ , which suggests the formation of a bulk low-dimensional material.

The chemical structure of graphyne was characterized with various analytical methods. To completely remove the molybdenum-based catalyst residue, the precipitate was washed with a large amount of THF and ammonium hydroxide solution. X-ray photoelectron spectroscopy confirmed that the molybdenum species was removed. Magic-angle spinning solid-state  $^{13}\text{C}$  NMR spectroscopy characterization supported the formation of graphyne as it showed the resonance signals at 140 ppm for the aromatic carbons and 100 ppm for the alkyne carbons. The relatively small peaks at 20 and 75 ppm were from the residual hexylphenylacetylene end groups (Supplementary Fig. 8). Thermogravimetric analysis showed that the  $\gamma$ -graphyne was thermally stable up to 250 °C with an 8% weight loss (Supplementary Fig. 9). X-ray diffraction analysis showed that the  $\gamma$ -graphyne had crystallinity after washing it with a variety of bench-top solvents, which included acetone, dichloromethane, THF, water and ammonium hydroxide solution. The sample did not show a considerable decrease of the crystallinity, even after soaking in boiling water, 1 M HCl or 1 M NaOH for 24 hours, which indicates the excellent stability of  $\gamma$ -graphyne (Supplementary Fig. 10).

Solid-state ultraviolet–visible–near infrared spectroscopy and cyclic voltammetry were conducted to estimate the bandgap.  $\gamma$ -Graphyne showed a broad absorption in the ultraviolet, visible and near infrared range (Supplementary Fig. 12). An optical bandgap was determined to be 0.96 eV using the Tauc method (Supplementary Fig. 13). Cyclic voltammetry showed a reduction potential of  $-0.95\ \text{V}$  versus  $\text{Ag}/\text{Ag}^+$  and an oxidation potential of

**Fig. 1 | Synthesis of  $\gamma$ -graphyne.** **a**, Structural relationship between  $sp^2$ -hybridized graphene and  $sp^2$ - and  $sp$ -hybridized  $\gamma$ -graphyne. **b**, Retrosynthetic analysis shows two possible routes to connect  $sp^2$  and  $sp$ -hybridized fragments: an irreversible cross-coupling reaction (X, halogen atoms) and a reversible alkyne metathesis reaction. The alkyne metathesis reaction entails the redistribution of alkyne bonds by scission and reconnection<sup>37</sup>. The two possible pathways of alkyne metathesis are illustrated using phenylpropyne as the substrate: in the non-productive pathway, phenylpropyne is regenerated, which resulted in no net change, and in the productive pathway diphenylacetylene and 2-butyne are formed. **c**, The synthesis of  $\gamma$ -graphyne from HPB and HHEB. 2-Butyne, 1-hexyl-4-(1-propyn-1-yl)-benzene and 2-bis(4-hexylphenyl)acetylene were produced as the by-products during the polymerization. Volatile 2-butyne was removed from the system, which drives the reaction towards the polymerization.



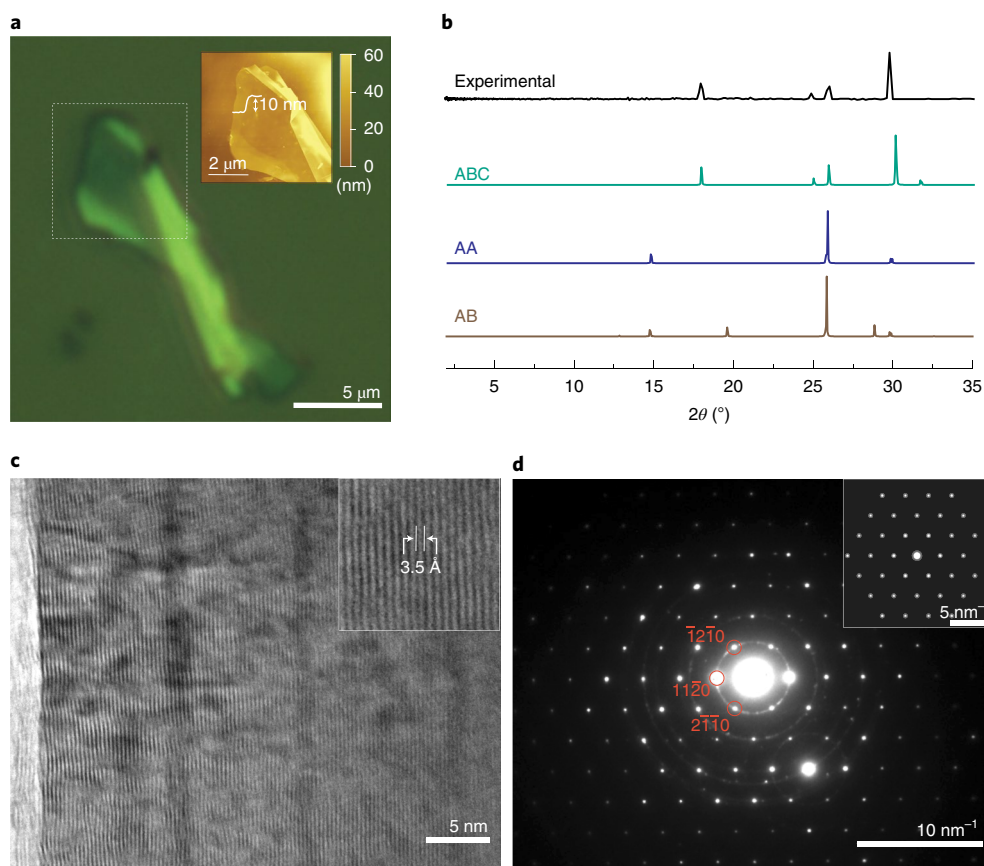


**Fig. 2 | Structural characterization of  $\gamma$ -graphyne.** **a**, Optical microscopy of the as-synthesized  $\gamma$ -graphyne on 100 nm  $\text{SiO}_2/\text{Si}$ . Inset: corresponding AFM image showing the step height. **b**, The experimental WAXS pattern of bulk  $\gamma$ -graphyne (black line) and calculated profiles of the simulated ABC, AA and AB stacking models. **c**, Lattice-resolution HRTEM image of  $\gamma$ -graphyne showing consistent lattice fringes, which are aligned vertically and parallel with the 0.35 nm spacing ( $d_{\{11\bar{2}0\}}$ ). **d**, The experimental SAED pattern of the as-synthesized  $\gamma$ -graphyne. Miller indices of representative crystal planes in accordance with the hexagonal representation of the ABC stacking model are shown. Inset: the calculated diffraction pattern from the  $\langle 001 \rangle$  direction.

$-0.02$  V versus  $\text{Ag}/\text{Ag}^+$  with an electronic bandgap of 0.93 eV. The material displayed a semiconductor band structure in which the highest occupied molecular orbital energy and lowest unoccupied molecular orbital energy were determined to be  $-4.78$  and  $-3.85$  eV, respectively, with ferrocene as the internal reference (Supplementary Figs. 14 and 15).

The bandgap of  $\gamma$ -graphyne was first predicted in 1987 by Baughman et al. to be 1.2 eV through the valence effective Hamiltonian technique<sup>13</sup>. Later, a few research groups reported the bandgap of  $\gamma$ -graphyne using different functionals in density functional theory calculations on unit-cell AA stacking models, typically in the range of 0.47–0.52 eV (refs. 42–44). We also calculated the bandgap of  $\gamma$ -graphyne based on the unit cells of the AA and ABC stacking models. Our calculation provided band gap values of 0.47 and 0.34 eV, respectively, for the AA and ABC stacking models (Supplementary Figs. 21 and 22), which agree well with the previously reported values. Our experimental bandgap of 0.93 eV is close to the value reported by Baughman et al.<sup>13</sup>, but larger than the typical predicted values based on density functional theory calculations<sup>42–44</sup>. Note that our experimental value is nearly three-fold smaller than the reported bandgap (2.7 eV) of the graphyne obtained through coupling of hexabromobenzene and calcium carbide<sup>32</sup>. As it is known that extended conjugation and delocalization of  $\pi$  electrons leads to low bandgaps in polymers<sup>44,45</sup>, it is expected that the  $\gamma$ -graphyne reported here has a higher polymerization degree than the hexabromobenzene-derived graphyne with an improved conjugation and fewer defects.

Wide-angle X-ray scattering (WAXS) characterization of the obtained  $\gamma$ -graphyne product suggests a unified crystalline structure. To confirm the structure observed from X-ray diffraction, we modeled the possible extended structures with different stacking methods, noted as AA (eclipsed), AB (partial staggered) and ABC (staggered) (Fig. 2b). The lattice constant  $a$  of the 2D lattice was estimated to be 0.69 nm through plane-wave density functional theory calculations. We found that the ABC stacking model matches well with the experimental profile, which shows the diffraction at  $2\theta = 18.01, 24.95, 26.09$  and  $29.87^\circ$ , which correspond to  $(10\bar{1}1)$ ,  $(10\bar{1}\bar{2})$ ,  $(11\bar{2}0)$  and  $(0003)$ , respectively. The intensive peak of the  $(0003)$  Bragg face indicates a long-range order in the vertical direction. To further validate the crystal structure of  $\gamma$ -graphyne, we performed high-resolution transmission electron microscopy (HRTEM) and selected-area electron diffraction (SAED) of a low-dimensional  $\gamma$ -graphyne sample. Owing to the thickness of these samples, electron diffraction analysis was mostly limited to the edges. A lattice-resolution HRTEM image of  $\gamma$ -graphyne shows consistent vertically aligned parallel lattice fringes of 0.35 nm (Fig. 2c), which correspond to  $d_{\{11\bar{2}0\}}$ . A hexagonal reciprocal lattice from the electron diffraction indicates the existence of  $C_6$  symmetry. As shown in Fig. 2d, the diffraction spots that are closest to the central transmission spot reveal a maximum plane spacing,  $d_{\text{max,SAED}} = 0.35$  nm, which matches well with the calculated diffraction pattern along the  $c$  axis (Fig. 2d, inset). To rule out any diffraction caused by the molybdenum residue, we also examined the HRTEM of the unwashed crude mixture from the control reaction

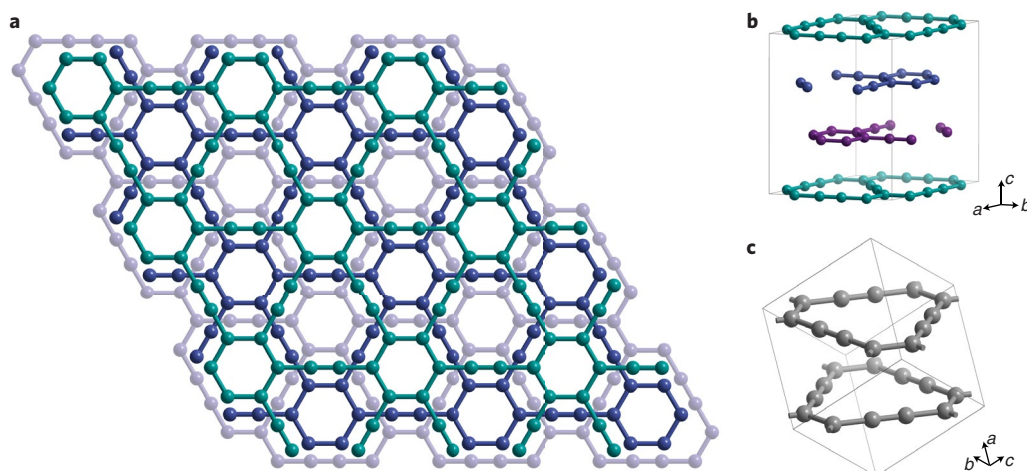


**Fig. 3 | Crystal structure of  $\gamma$ -graphyne with the unit cell and primitive cell. a**, Structure of  $\gamma$ -graphyne layers. **b**, Hexagonal representation of the  $\gamma$ -graphyne unit cell, with the crystal axes denoted. **c**, Rhombohedral representation of the  $\gamma$ -graphyne primitive cell, with the crystal axes denoted.

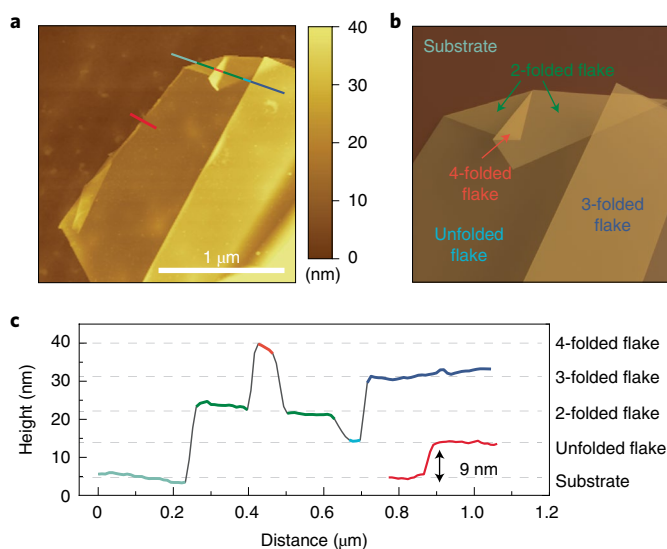


**Fig. 4 | Folding behaviour of  $\gamma$ -graphyne. a**, AFM image of the exfoliated and folded  $\gamma$ -graphyne thin film. **b**, Illustration of the folding behaviours that correspond to the image in **a**. **c**, A height plot of the layered structure of exfoliated  $\gamma$ -graphyne. The red line indicates the thickness of the exfoliated thin flake; the multicoloured line indicates the step changes due to the folding mechanism.

without the added alkyne monomer. This showed a square lattice with a spacing of 0.25 nm, which is distinct from that observed for  $\gamma$ -graphyne (Supplementary Fig. 19).

Next, a detailed investigation of the correlation between the experimental profile and the calculated profile of ABC stacking was made based on the optimized crystal structure of the  $\gamma$ -graphyne ABC stacking model. As shown in Fig. 3, the ABC stacking model is of a no. 166  $R\bar{3}M$  space group in a hexagonal lattice. Apart from its characteristic hexagonal unit cell (Fig. 3b), the no. 166 space group can be simplified via a rhombohedral representation as the primitive cell (Fig. 3c), which indicates an intrinsic ‘bilayer stacking’ nature within the ABC stacking mode. By comparing both profiles, we assigned each peak of the experimental profile to the Miller indices of the crystal planes in accordance with both the hexagonal representation and the rhombohedral representation as:  $18.0^\circ$  ( $d=0.49$  nm,  $(10\bar{1}1)$  and  $(00\bar{1})$ ),  $25.0^\circ$  ( $d=0.36$  nm,  $(10\bar{1}2)$  and

$(0\bar{1}\bar{1})$ ),  $25.9^\circ$  ( $d=0.34$  nm,  $(11\bar{2}0)$  and  $(10\bar{1}\bar{1})$ ) and  $30.1^\circ$  ( $d=0.30$  nm,  $(0003)$  and  $(111)$ ). Revealing the ABC stacked  $\gamma$ -graphyne superlattice increases the understanding of the formation of such 2D material and could help guide future theoretical study and experimental development of this uncharted class of materials.

The exfoliated films exhibited layered height profiles commensurate with step edges within a single flake with a height of 9 nm (Fig. 4a, red line). Unprecedentedly, a folding behaviour was observed on exfoliation of the  $\gamma$ -graphyne thin film. The multicoloured line in Fig. 4a outlines the height profile of a  $\gamma$ -graphyne flake, showing its folded state. The detailed folding manner is depicted in Fig. 4b, in which the main sheet folded onto itself, with a range from double-step to tetra-step folding. The height profile shown in Fig. 4c is consistent with a single step of 9 nm.

## Conclusion

We demonstrated the synthesis of  $\gamma$ -graphyne in bulk by utilizing a dynamic alkyne metathesis reaction. A meticulous balance between kinetic and thermodynamic control was managed through the simultaneous use of two different hexa-alkynyl-substituted benzenes as the comonomers to yield crystalline  $\gamma$ -graphyne. Furthermore, its interlayer ABC stacking mode was revealed through bulk X-ray diffraction and few-layer electron diffraction in both the macro- and microscale. We also observed the sheet-like morphology of  $\gamma$ -graphyne and its folding behaviour. Understanding such folding behaviour will open many possibilities to explore the unique mechanical and electronic properties of this periodically  $sp$ - $sp^2$ -hybridized  $\gamma$ -graphyne, an intriguing new member added to the 2D material family.

## Methods

$\gamma$ -Graphyne was synthesized under an argon atmosphere. The molybdenum precursor and ligand were synthesized following a literature procedure<sup>41</sup>. The molybdenum precursor, ligand, HPB, HHEB, stir bar and Schlenk tube were dried to remove moisture. The molybdenum precursor (3.2 mg, 0.005 mmol) and ligand (2.3 mg, 0.005 mmol) were put into a 10 ml Schlenk tube charged with  $\text{CCl}_4$  (0.5 ml). The mixture was stirred at  $70^\circ\text{C}$  for 30 min under an argon atmosphere. HPB (22.0 mg, 0.072 mmol) and HHEB (8.6 mg, 0.008 mmol) dissolved in 2.5 ml of  $\text{CCl}_4$  were added to the above activated catalyst solution. The tube was placed at 77 K in a liquid nitrogen bath until the  $\text{CCl}_4$  was just frozen, then evacuated and sealed at a pressure of around 10 mtorr. The tube was placed in a  $70^\circ\text{C}$  oil bath without any disturbance. After 1, 3, 5, 8, 12 and 24 h, the tube was frozen, evacuated to remove the 2-butyne by-product and resealed at a pressure of around 10 mtorr. After 3 days, a dark black solid precipitated out. The product was washed with a large excess of THF ( $3 \times 15$  ml) and then ammonium hydroxide solution ( $3 \times 5$  ml) to remove the by-products, oligomers and the catalyst residue to provide  $\gamma$ -graphyne (6.3 mg, 72%).

**Data availability**

Experimental data and characterization data are provided in the Supplementary Information. Crystallographic data for the structure HPB reported in this Article has been deposited at the Cambridge Crystallographic Data Centre (CCDC), under deposition number 2111647. Copies of the data can be obtained free of charge via <https://www.ccdc.cam.ac.uk/structures/>.

Received: 3 November 2021; Accepted: 25 March 2022;

Published online: 09 May 2022

**References**

- Kroto, H. W., Heath, J. R., O'Brien, S. C., Curl, R. F. & Smalley, R. E. C60: buckminsterfullerene. *Nature* **318**, 162–163 (1985).
- Iijima, S. Helical microtubules of graphitic carbon. *Nature* **354**, 56–58 (1991).
- Novoselov, K. S. et al. Electric field effect in atomically thin carbon films. *Science* **306**, 666–669 (2004).
- Fan, Q. et al. Biphenylene network: a nonbenzenoid carbon allotrope. *Science* **372**, 852–856 (2021).
- Kaiser, K. et al. An *sp*-hybridized molecular carbon allotrope, cyclo[18]carbon. *Science* **365**, 1299–1301 (2019).
- Malko, D., Neiss, C., Viñes, F. & Görling, A. Competition for graphene: graphynes with direction-dependent Dirac cones. *Phys. Rev. Lett.* **108**, 086804 (2012).
- Chen, J., Xi, J., Wang, D. & Shuai, Z. Carrier mobility in graphyne should be even larger than that in graphene: a theoretical prediction. *J. Phys. Chem. Lett.* **4**, 1443–1448 (2013).
- Kang, J., Li, J., Wu, F., Li, S.-S. & Xia, J.-B. Elastic, Electronic, and Optical Properties of Two-Dimensional Graphyne Sheet. *J. Phys. Chem. C* **115**, 20466–20470 (2011).
- Peng, Q., Ji, W. & De, S. Mechanical properties of graphyne monolayers: a first-principles study. *Phys. Chem. Chem. Phys.* **14**, 13385–13391 (2012).
- Cranford, S. W. & Buehler, M. J. Mechanical properties of graphyne. *Carbon* **49**, 4111–4121 (2011).
- Zhang, Y. Y., Pei, Q. X. & Wang, C. M. Mechanical properties of graphynes under tension: a molecular dynamics study. *Appl. Phys. Lett.* **101**, 081909 (2012).
- Hirsch, A. The era of carbon allotropes. *Nat. Mater.* **9**, 868–871 (2010).
- Baughman, R. H., Eckhardt, H. & Kertesz, M. Structure–property predictions for new planar forms of carbon: layered phases containing *sp*<sup>2</sup> and *sp* atoms. *J. Chem. Phys.* **87**, 6687–6699 (1987).
- Kehoe, J. M. et al. Carbon networks based on dehydrobenzoannulenes. 3. Synthesis of graphyne substructures. *Org. Lett.* **2**, 969–972 (2000).
- Johnson, C. A., Lu, Y. & Haley, M. M. Carbon networks based on benzocyclynes. 6. Synthesis of graphyne substructures via directed alkyne metathesis. *Org. Lett.* **9**, 3725–3728 (2007).
- Haley, M. M. Synthesis and properties of annulenic subunits of graphyne and graphdiyne nanoarchitectures. *Pure Appl. Chem.* **80**, 519–532 (2008).
- Kilde, M. D. et al. Synthesis of radiannulene oligomers to model the elusive carbon allotrope 6,6,12-graphyne. *Nat. Commun.* **10**, 3714 (2019).
- Gao, Y. et al. The loss of endgroup effects in long pyridyl-encapped oligoynes on the way to carbyne. *Nat. Chem.* **12**, 1143–1149 (2020).
- Eisler, S. & Tykwinski, R. R. Expanded radialenes: modular synthesis and characterization of cross-conjugated enyne macrocycles. *Angew. Chem. Int. Ed.* **38**, 1940–1943 (1999).
- Tahara, K. et al. Syntheses and properties of graphyne fragments: trigonally expanded dehydrobenzo[12]annulenes. *Chem. Eur. J.* **19**, 11251–11260 (2013).
- Tahara, K. et al. Control and induction of surface-confined homochiral porous molecular networks. *Nat. Chem.* **3**, 714–719 (2011).
- Tahara, K., Yoshimura, T., Ohno, M., Sonoda, M. & Tobe, Y. Syntheses and photophysical Properties of boomerang-shaped bis(dehydrobenzo[12]annulene) and trapezoid-shaped tris(dehydrobenzo[12]annulene). *Chem. Lett.* **36**, 838–839 (2007).
- Zhang, W., Brombosz, S. M., Mendoza, J. L. & Moore, J. S. A high-yield, one-step synthesis of *o*-phenylene ethynylene cyclic trimer via precipitation-driven alkyne metathesis. *J. Org. Chem.* **70**, 10198–10201 (2005).
- Diederich, F. & Kivala, M. All-carbon scaffolds by rational design. *Adv. Mater.* **22**, 803–812 (2010).
- Grave, C. & Schlüter, A. D. Shape-persistent, nano-sized macrocycles. *Eur. J. Org. Chem.* **2002**, 3075–3098 (2002).
- Zhang, W. & Moore, J. S. Shape-persistent macrocycles: structures and synthetic approaches from arylene and ethynylene building blocks. *Angew. Chem. Int. Ed.* **45**, 4416–4439 (2006).
- Li, G. et al. Architecture of graphdiyne nanoscale films. *Chem. Commun.* **46**, 3256–3258 (2010).
- Li, Y., Xu, L., Liu, H. & Li, Y. Graphdiyne and graphyne: from theoretical predictions to practical construction. *Chem. Soc. Rev.* **43**, 2572–2586 (2014).
- Huang, C. et al. Progress in research into 2D graphdiyne-based materials. *Chem. Rev.* **118**, 7744–7803 (2018).
- Pan, Q. et al. Direct synthesis of crystalline graphtetrayne—a new graphyne allotrope. *CCS Chem.* **3**, 1368–1375 (2021).
- Li, Q. et al. Synthesis of  $\gamma$ -graphyne by mechanochemistry and its electronic structure. *Carbon* **136**, 248–254 (2018).
- Li, Q., Yang, C., Wu, L., Wang, H. & Cui, X. Converting benzene into  $\gamma$ -graphyne and its enhanced electrochemical oxygen evolution performance. *J. Mater. Chem. A* **7**, 5981–5990 (2019).
- Ding, W., Sun, M., Zhang, Z., Lin, X. & Gao, B. Ultrasound-promoted synthesis of  $\gamma$ -graphyne for supercapacitor and photoelectrochemical applications. *Ultrason. Sonochem.* **61**, 104850 (2020).
- Diederich, F. Carbon scaffolding: building acetylenic all-carbon and carbon-rich compounds. *Nature* **369**, 199–207 (1994).
- Cao, Y. et al. Unconventional superconductivity in magic-angle graphene superlattices. *Nature* **556**, 43–50 (2018).
- Zhou, H., Xie, T., Taniguchi, T., Watanabe, K. & Young, A. F. Superconductivity in rhombohedral trilayer graphene. *Nature* **598**, 434–438 (2021).
- Fürstner, A. The ascent of alkyne metathesis to strategy-level status. *J. Am. Chem. Soc.* **143**, 15538–15555 (2021).
- Ma, T. et al. Single-crystal X-ray diffraction structures of covalent organic frameworks. *Science* **361**, 48–52 (2018).
- Hu, Y. et al. Single crystals of mechanically entwined helical covalent polymers. *Nat. Chem.* **13**, 660–665 (2021).
- Jin, Y. H., Yu, C., Denman, R. J. & Zhang, W. Recent advances in dynamic covalent chemistry. *Chem. Soc. Rev.* **42**, 6634–6654 (2013).
- Du, Y. et al. Highly active multidentate ligand-based alkyne metathesis catalysts. *Chem. Eur. J.* **22**, 7959–7963 (2016).
- Narita, N., Nagai, S., Suzuki, S. & Nakao, K. Optimized geometries and electronic structures of graphyne and its family. *Phys. Rev. B* **58**, 11009–11014 (1998).
- Zhou, J. et al. Electronic structures and bonding of graphyne sheet and its BN analog. *J. Chem. Phys.* **134**, 174701 (2011).
- Srinivasu, K. & Ghosh, S. K. Graphyne and graphdiyne: promising materials for nanoelectronics and energy storage applications. *J. Phys. Chem. C* **116**, 5951–5956 (2012).
- Scharber, M. C. & Sariciftci, N. S. Low band gap conjugated semiconducting polymers. *Adv. Mater. Technol.* **6**, 2000857 (2021).

**Acknowledgements**

We thank J. Choi (University of Colorado Boulder) for helpful discussions on the electrochemistry tests and B. Lama (University of Colorado Boulder) for solid-state NMR spectroscopy data acquisition. W.Z. acknowledges the National Science Foundation (DMR-1420736). Y.Z. acknowledges the National Natural Science Foundation of China (31202117). Y.H. thanks the Summer Graduate Fellowship support from University of Colorado Boulder. We thank the Soft Materials Research Center for use of the WAXS instrument with support from the National Science Foundation (DMR-1420736).

**Author contributions**

Y.H., Y.Z. and W.Z. conceived the idea and led the project. Y.H., S.H., J.W. and L.J.W. conducted the synthesis. C.W. conducted the modelling. Q.P. and Y.Z. conducted the transmission electron microscopy. R.L. and M.B.R. conducted the AFM. V.M. and N.A.C. conducted the WAXS. Y.H., Y.J., Y.Z. and W.Z. interpreted the results and Y.H., Y.J. and W.Z. wrote the manuscript.

**Competing interests**

Y.H. and W.Z. are inventors on a US patent application submitted by University of Colorado Boulder. The other authors do not have any competing interests.

**Additional information**

**Supplementary information** The online version contains supplementary material available at <https://doi.org/10.1038/s44160-022-00068-7>.

**Correspondence and requests for materials** should be addressed to Yingjie Zhao or Wei Zhang.

**Peer review information** *Nature Synthesis* thanks the anonymous reviewers for their contribution to the peer review of this work. Primary Handling editor: Peter Seavill, in collaboration with the *Nature Synthesis* team.

**Reprints and permissions information** is available at [www.nature.com/reprints](http://www.nature.com/reprints).

**Publisher's note** Springer Nature remains neutral with regard to jurisdictional claims in published maps and institutional affiliations.

© The Author(s), under exclusive licence to Springer Nature Limited 2022